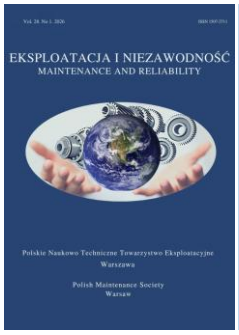

Eksploatacja i Niezawodnosc – Maintenance and Reliability

Volume 28 (2026), Issue 1

journal homepage: http://www.ein.org.pl

Article citation info:
Zhang K, Yang G Yang M, Ma C, Xu Y, LSESgram: A novel approach for optimal demodulation band selection in rolling bearing fault diagnosis, Eksploatacja i Niezawodnosc – Maintenance and Reliability 2026: 28(1) http://doi.org/10.17531/ein/208154

LSESgram: A novel approach for optimal demodulation band selection in rolling bearing fault diagnosis

Indexed by: Web of Science Group

Kun Zhang[a], Guangshuai Yang[a], Miaorui Yang[a,*], Chaoyong Ma[a], Yonggang Xu[a]

[a] Beijing University of Technology, China

Highlights

- This paper proposes LSESgram for optimal frequency modulation band selection.
- LSESgram is robust to noise and interference,which struggle under noisy conditions.
- LSESgram validated via simulations,experiments, beats Fast Kurtogram, Infogram, Autogram.

Abstract

Envelope demodulation has become a key technique in rolling bearing fault diagnosis. However, selecting the optimal frequency modulation band that captures rich fault information remains a challenge, especially in the presence of low signal-to-noise ratios, accidental pulses, and irrelevant harmonics. This paper presents a novel approach, LSESgram, for optimal frequency modulation band selection. Unlike existing methods such as Spectral Kurtosis and Kurtogram, which struggle under noisy conditions, LSESgram is robust to noise and interference. It first extracts spectral trends using a scale-space-like theory, then performs multi-level segmentation based on these trends. The LSES indicator is then used to identify the optimal demodulation frequency band. The method is validated with simulation and experimental signals, showing superior performance compared to Fast Kurtogram, Infogram, and Autogram.

Keywords
fault diagnosis, rolling bearing, L-kurtosis, LSES, optimal frequency modulation band, LSESgram

1. Introduction

With the increasing automation of rotating machinery, fault diagnosis techniques are receiving increasing attention. Bearings are one of the most important components of various rotating machines [1], and their operating conditions. Once we fail to detect and eliminate weak faults in time, it may lead to damage of the bearing itself as well as the whole equipment, which in turn may cause serious economic losses in the continuous production activities of the industry [2]. Therefore, bearing fault diagnosis is crucial for assessing the operational status of mechanical equipment and preventing accidents [3-5].

Bearings may experience variable and constant speeds during normal operation, and it is easier to find fault information about a faulty bearing under constant speed conditions [6]. Under constant speed conditions, when damage occurs at a specific location in the bearing, the rolling element will repeatedly strike the damaged area and generate periodic pulses. The resulting pulses contain complex high-frequency components, which cause the sensors or components of the system to be excited to resonate. Demodulation of the signal in the resonant band range of the system results in a lower frequency envelope signal with a higher signal-to-noise ratio [7], and the fault characteristic frequencies are more easily observed. Among the many fault diagnosis techniques, adaptive decomposition and sparse signal representation are widely used. Among which overcomplete

(*) Corresponding author.
E-mail addresses: K. Zhang (ORCID: 0000-0002-3513-8988) zkun212@163.com, G. Yang (ORCID: 0009-0005-3162-5243) yangguangshuai@163.com, M Yang (ORCID: 0000-0002-0006-4288) yangmiaorui@163.com, C. Ma (ORCID: 0000-0001-9109-891X) machaoyong_bjut@163.com, Y. Xu (ORCID: 0000-0002-2206-8968) xyg_1975@163.com,

dictionaries for sparse signal representation can be categorized as analytic dictionaries and learning dictionaries. Analytic dictionaries have a fixed structure with limited adaptability. Adaptive decomposition can partition the signal into multiple narrowband components, aiding in the quantitative assessment of signal characteristics. Nonetheless, this method incurs high computational complexity, prolonged processing time, and increased cost. envelope analysis, also known as the resonance demodulation technique, is widely used today [8]. The resonant bands in the spectrum are first discovered and the corresponding filtered signals are obtained, and then the envelope spectrum analysis is performed to observe the fault characteristic frequencies present in them. However, how to accurately extract the resonant bands has been the main challenge of such methods.

Dwyer [9] first introduced the concept of spectral kurtosis (SK) as a statistical tool to measure the non-Gaussian components in a signal and to locate non-Gaussian components in the frequency domain.SK characterizes the magnitude of the kurtosis of each spectral line in the signal's frequency domain and describes the distribution of the kurtosis with frequency. Then, based on the Wold-Cramer decomposition theory, Antoni [10] explained SK systematically and proposed a complete theoretical system of SK applicable to non-stationary signals, defining it as a normalized fourth-order accumulation of energy. He further studied the application of SK with Randall [11], proposing Fast Kurtogram based on the short-time Fourier transform, but the method is computationally expensive, which is not conducive to engineering applications. Later, Antoni [12] proposed Fast Kurtogram based on a Finite Pulse Response (FIR) filter, which greatly improved the computational efficiency and practicality of the SK method. However, Fast Kurtogram ignores the different characteristics of the fault vibration signal and may fail when the noise in the signal is strong [13]. Subsequently, many scholars have proposed improvements to Fast Kurtogram. Lei [14] used wavelet packet decomposition instead of a FIR filter in Fast Kurtogram, thus reducing the effect of noise and obtaining higher accuracy of spectrum division.

Barszcz and Jablonski found that SK fails in the presence of high amplitude non-Gaussian noise in the signal. To overcome these drawbacks, they proposed a method based on the envelope spectral kurtosis rather than the filter time signal kurtosis, namely Protrugram [15]. It requires the use of a filter three times the width of the fault frequency to scan the entire frequency band. Wang [16] used the wavelet packet transform for multilevel segmentation of the spectrum and the proposed Sparsogram for amplifying the information in the signal. Antoni [17] was inspired by the concept of entropy in thermodynamics and argued that the entropy of the signal changes during transient pulses. Therefore, he proposed the Infogram to calculate the negative entropy of the signal [18]. He defined the SE Infogram, which is based on the negative entropy of the signal's square envelope, the SES Infogram, which is based on the negative entropy of the signal's square envelope spectrum, and the Average Infogram, which is based on the weighted average of the two, to detect repeated transients. Recently, Moshrefzadeh and Fasana [19] developed Autogram, which uses the unbiased autocorrelation kurtosis of the signal squared envelope as an evaluation index to improve the reliability of the optimal demodulation band selection for rolling bearing vibration signals. Since the autocorrelation function is introduced, the effect of random pulse noise can be weakened and the periodic components in the vibration signal can be captured effectively. Wang [20] developed the TIEgram, which weighted the fusion of the kurtosis, correlation coefficient, and spectral negative entropy to improve the reliability of the optimal demodulation band selection indicator. However, the existing optimal demodulation band selection methods still have shortcomings. First, the traditional binary tree or 1/3 binary tree segmentation models used in some methods segment the spectrum mechanically and cannot segment it according to the shape of the signal spectrum itself, which has the disadvantage of insufficient segmentation accuracy. Second, some methods do not perform well when dealing with signals containing incidental pulses and extraneous harmonic interference. Third, some methods require parameter presetting based on a priori knowledge, which reduces the efficiency of diagnosis.

The traditional binary tree or 1/3 binary tree segmentation methods mentioned above cannot segment the spectrum according to its inherent shape. To address this limitation, this paper employs the key function method from the theory of scale space to extract spectral trends with different levels of granularity and performs multi-layer segmentation to better

align with the inherent shape of the spectrum. To overcome the poor performance of previous methods in handling occasional pulses and external harmonic interference, this paper introduces a novel algorithm—LSESgram. By calculating the LSES value of the extracted spectral components, an LSESgram is generated. The frequency band with the maximum LSES value is then identified and its fault characteristics are further extracted for fault diagnosis. In this paper, we use LSESgram to process the simulated and experimental signals and compare the results with Fast Kurtogram, Infogram, and Autogram to verify the superiority of the proposed method. The comparison results show that LSESgram has good results in processing bearing fault signals containing strong noise, chance pulses, and irrelevant harmonics. This paper is structured as follows: Section II describes the cancellation process of the incidental pulse and extraneous harmonic disturbances provides a theoretical description and characterization of LSESgram indicator and describes the specific steps of LSESgram. In Section III, the simulated signal analysis is performed for LSESgram. In Section IV, LSESgram is applied to the experimental signals, and the results are compared with Fast Kurtogram, Infogram, and Autogram. Section 5 concludes the paper.

2. Theoretical elaboration

2.1. Elimination of accidental pulses and extraneous harmonic disturbances

When a rolling bearing fails, the signal envelope spectrum will have the failure frequency of the corresponding component and its multiples. Ideally, this can be seen as a series of repetitive transients of different amplitudes, and these repetitive transients are also a series of repetitive transients of different periods in the frequency domain of the envelope, which are expressed as Dirac comb functions. Therefore, if there are fault frequencies and their multiples in the envelope spectrum, there should be similar Dirac comb functions in its amplitude spectrum, and vice versa, which means that the amplitude spectrum of the envelope spectrum can also be used as the computational domain of statistical indicators.

A simple model of periodic pulse signals under a single degree of freedom forcibly vibrating system with damping is constructed as follows:

$$p(t) = \sum_{-\infty}^{\infty} Ae^{-2\pi\zeta f_n t}\delta(t - nT_0) \quad (1)$$

where ζ is the damping ratio, $f_n$is the intrinsic frequency, $T_0$is the period, n is an integer, $n = 0, \pm1, \pm2, \cdots$, A is the amplitude of the periodic pulse.

Under the same system, the simple model of a single non-periodic instantaneous pulse signal is:

$$g(t) = Ce^{-2\pi\zeta f_n t}\delta(t - t_0) \quad (2)$$

where t_0 is a certain moment, and C is the amplitude of the non-periodic instantaneous pulse.

The periodic pulse signal containing a single nonperiodic instantaneous pulse is the superposition of two signals, and the expression is：

$$s(t) = \sum_{-\infty}^{\infty} Ae^{-2\pi\zeta f_n t}\delta(t - nT_0) + Ce^{-2\pi\zeta f_n t}\delta(t - t_0) \quad (3)$$

The analytic signal h(t) of the signal $s(t)$ is obtained by the Hilbert transform.

$$h(t) = x(t) + H[x(t)] = p(t) + g(t) + jH[p(t) + g(t)]$$
$$= p(t) + jH[p(t)] + g(t) + jH[g(t)] = h_p(t) + h_g(t) \quad (4)$$

Then the envelope signal of signal $s(t)$ is：

$$E(t) = \left|h_p(t)\right| + \left|h_g(t)\right| \quad (5)$$

The Fourier transform is performed on the envelope signal to obtain the envelope spectrum. According to the linear superposition property, the envelope spectrum of the signal $s(t)$ is:

$$ES(f) = FT[E(t)] = FT\left[\left|h_p(t)\right|\right] + \left[\left|h_g(t)\right|\right]$$
$$= ES_p(f) + ES_g(f) \quad (6)$$

Refer to (6), it can be seen that the envelope spectrum of a periodic pulse signal containing a single nonperiodic instantaneous pulse is equivalent to the result of superimposing the envelope spectra of two signals.

The envelope spectrum of a single non-periodic instantaneous pulse signal is a curve that gradually decays in amplitude as the frequency increases. After superimposing with the envelope spectrum of a periodic pulse signal, the spectral lines near the origin of the envelope spectrum of a periodic pulse signal appear to be elevated, changing the arrangement of the spectral lines in the envelope spectrum of a periodic pulse signal.

The Fourier transform calculation of the envelope spectrum is equivalent to finding the spectrum of the envelope spectrum as follows.

$$SES = \left|FT\left[ES_p(f) + ES_g(f)\right]\right|$$
$$= \left|FT[ES_p(f)]\right| + \left|FT[ES_g(f)]\right| \quad (7)$$

In the amplitude spectrum of the envelope spectrum, the spectral line representing a single non-periodic transient pulse signal is located near the origin and is approximately parallel to the vertical axis. If low-pass filtering is performed in the spectrum of the envelope, the non-periodic components can be directly eliminated, and to simplify the process, the components near the origin can be directly defined as 0.

Fig.1(a)-(b) shows the constructed outer ring fault simulation signal and its envelope waveform containing a single non-periodic transient pulse, respectively. The non-periodic transient pulse will disturb not only the fault signal but also its envelope waveform. When the acquired signal contains a single incidental pulse, it causes a steep and large increment in the envelope spectrum of the acquired signal, which is manifested in the envelope spectrum as the spectral line lifts along the vertical axis, which causes the shape of the envelope spectrum to be changed, as shown in Fig. 1(c). Further calculation of the frequency spectrum of the envelope spectrum, as shown in Fig. 1(d), reveals that the amplitude spectrum has a steep rise at the origin and the endpoint, thus reflecting the occasional and periodic pulses in the time domain signal into the amplitude spectrum of the envelope spectrum. If further low-pass filtering (the low-pass filtering length is 2%-3% of the sampling points) is performed to filter out the steep rise in amplitude, the effect of the incidental pulses can be eliminated and only the periodic components are retained, and the effect is similar to that of part B in Fig. 1(d). Similarly, the signal with harmonic interference can be eliminated by this method to eliminate the interference of irrelevant harmonics. Fig. 1(e)-(f) show enlarged views of A and B in Fig. 1(d), respectively. The signal $p(t)$ is:

$$p(t) = 10 \cdot e^{-700 \cdot mod\left(\frac{n}{F_S} - 0.43, \frac{1}{1}\right)} \cdot sin\left(2\pi \cdot \frac{n \cdot 1500}{F_S}\right) + 0.6 \cdot e^{-900 \cdot mod\left(\frac{n}{F_S}, \frac{1}{80}\right)} \cdot sin\left(2\pi \cdot \frac{n \cdot 2400}{F_S}\right) \quad (8)$$

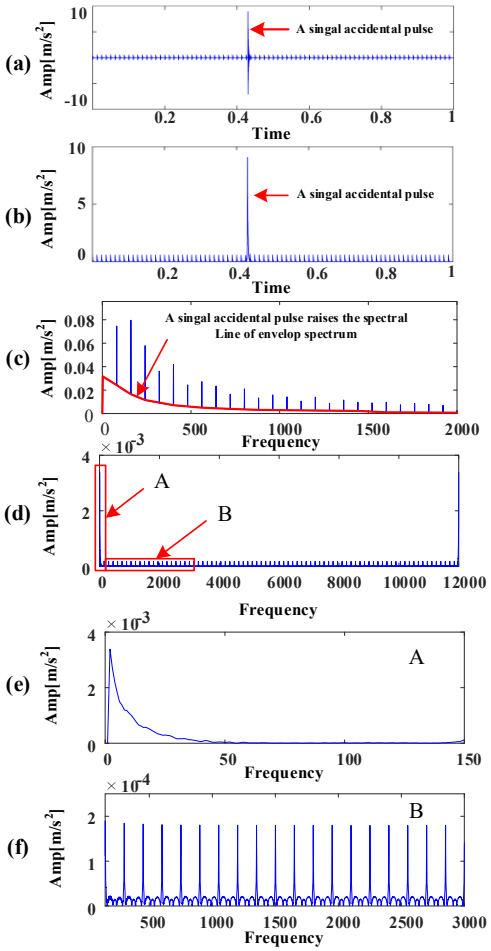

Fig. 1. (a) The time domain waveform; (b) The envelope waveform; (c) The Envelope spectrum; (d) The amplitude spectrum of the envelope spectrum; (e) Zoomed-in view at A in the envelope spectrum; (f) Zoomed-in view at B in the envelope spectrum.

2.2. Optimal demodulation band selection indicator: LSES

Hosking [21] introduced the concept of L-moments based on the statistical theory of order. For a sequence of continuous random variables {X} with r-order L-moments, the sequence of order $X_{1:r} \le X_{2:r} \le \cdots \le X_{r:r}$, can be obtained by the magnitude of the values. Then the linear moment of the sequence of random variables is:

$$\lambda_r = \frac{1}{r} \cdot \sum_{k=0}^{r-1} (-1)^j \cdot C_k^{r-1} E(X_{r-k:r}), r = 1,2,\cdots \quad (9)$$

where C_k^{r-1} is the number of combinations obtained by selecting k variables from $r-1$ random variables ,$X_{r-k:r}$ is the $(r-k)$ th smallest random variable, $E[X_{r-k:r}]$ is the mathematical expectation of the random variable.

The order r of the sequence of random variables is the length $r$of the sequence.

The expectation of the rth order statistic for a sequence of arbitrary length n is:

$$E(X_{r:n}) = \frac{n!}{(r-1)!\cdot(n-r)!}\cdot\int_0^1 x(F)\cdot[F(x)]^{r-1}\cdot[1-F(x)]^{n-r}dF(x) \quad (10)$$

Therefore, the first fourth-order L-moments can be obtained from Eq. (8) and Eq. (9) as follows:

$$\begin{cases}\lambda_1 = E(X_{1:1}) = b_0\\ \lambda_2 = \frac{1}{2}E(X_{2:2}-X_{1:2}) = 2b_1 - b_0\\ \lambda_3 = \frac{1}{3}E(X_{3:3}-2X_{2:3}+X_{1:3}) = 6b_2 - 6b_1 + b_0\\ \lambda_4 = \frac{1}{4}E(X_{4:4}-3X_{3:4}+3X_{2:4}-X_{1:4})\end{cases} \quad (11)$$

where $b_i = \int_0^1 x(F)\cdot[F(x)]^i dF(x), i = 0,1,2,3$ is the ith order probability moment.

According to the definition of linear moment, the first-order L-moment λ_1 represents the mean of the random sequence, while the second-order L-moment λ_2 can be interpreted as the dispersion of the distribution of the random sequence, similar to the variance of the constant rule. The L-kurtosis (LK) is defined as:

$$LK = \frac{\lambda_4}{\lambda_2} \quad (12)$$

The L-moments of a random signal can be calculated as long as the expectation of the signal exists. Compared with the normal rule, linear moments can be estimated unbiased by linear combinations of sampled values and are more resistant to interference. In particular, for outliers in the data, linear moments are more robust than the normal rule, giving better results with a smaller number of samples.

Let $ES(f)$ denote the envelope spectrum, for which the Fourier transform is calculated to obtain its amplitude spectrum as:

$$SES = |FT[ES(f)]| \quad (13)$$

The physical meaning of the spectrum of the envelope is not elaborated in this paper, so the horizontal coordinate of the spectrum of the envelope is defined as the number of sampling points. To reduce the effects of accidental pulses and extraneous harmonic interference, the components of the spectrum of the envelope near the origin are defined as 0. By calculating the LK of the amplitude spectrum of the envelope spectrum, this paper proposes the concept of the LSES as indicator which can be represented as:

$$LSES = \frac{\lambda_4(SES)}{\lambda_2(SES)} \quad (14)$$

2.3. Characterization of the LSES indicator

To demonstrate that the LSES indicator is not easily disturbed by accidental pulses and extraneous harmonics, four sets of simulated signals with 2000 sample points were constructed for verification, as shown in Fig. 2(a). They are random noise signal (Sig. 1), sinusoidal harmonic signal (Sig. 2), single pulse signal (Sig. 3), and periodic pulse signal (Sig. 4). The LSES of the five signals are calculated as shown in Fig. 2(b). It can be clearly observed that the LSES value of sig.4 is the largest. This indicates that the LSES indicator is more sensitive to periodic pulse components. Fig. 2 suggests that the LSES indicator has the ability to characterize whether the signal contains a periodic component that is critical for measuring failure information in rolling bearings.

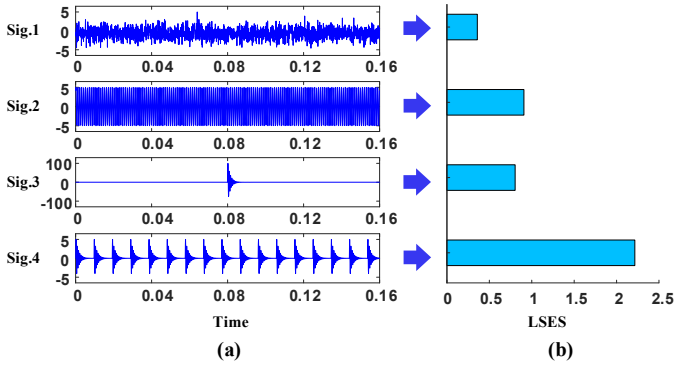

Fig. 2. The degree of reflection of different signals by LSES: (a) Simulated signals 1-4; (b) LSES of simulated signals 1-4.

To further express the LSES to measure the periodicity of the signal and its ability to resist noise, the variation of the LSES with the number of pulses under different noise conditions is investigated. For a signal of finite length, the number of pulses is an important factor in evaluating the pulse characteristics of the signal. A series of periodic pulse signals with different numbers of pulses and amplitude of 1 are constructed and white noise is added to form a periodic pulse simulation signal with different noise variances. According to Fig. 3, we compared LSES with kurtosis and L-kurtosis. In Fig. 3(a), the kurtosis decreases with increasing number of pulses, which is consistent with the characteristics of kurtosis. Compared to L-kurtosis,

LSES can characterize the presence or absence of periodic components in a signal at a smaller number of pulses. In terms of noise immunity, LSES has better noise immunity. As shown in the boxed areas in Fig. 3(b) and Fig. 3(c), the growth area of LSES is larger when the noise variance is 0.05 and 0.1, which indicates that LSES is less susceptible to noise than L-kurtosis. In summary, LSES has excellent periodic component characterization capability and noise immunity and is well suited for fault feature extraction of rolling bearings.

2.4. LSESgram

In this section, an optimal band selection method that can resist strong noise as well as accidental pulse and harmonic interference, LSESgram, is proposed. Firstly, multiple spectral trends are obtained, then the location of the minima of the spectrum trend is used as the boundary to segment the original spectrum, and then decompose the signals into a series of empirical modal components. Finally, calculate the LSES value of each component and select the component with the largest LSES value for demodulation analysis for fault diagnosis, which is the basic content of LSESgram. The main steps of LSESgram are as follows.

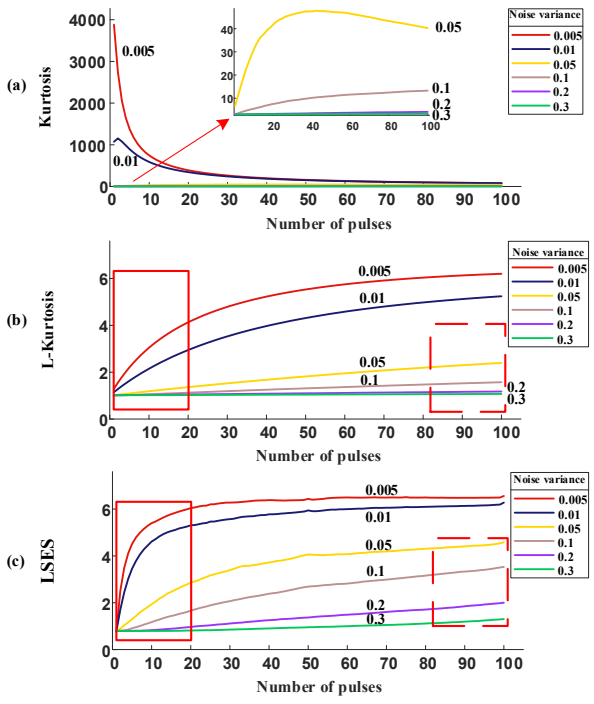

Fig. 3. Variation of (a) kurtosis; (b) L-kurtosis; (c) LSES with the number of pulses under different noise conditions.

Step 1: Extract the spectral trend by using the key function method of scale-space-like theory. The scale space theory is a method of convolving the original signal with a kernel function containing variable scale parameters and then realizing filtering. In layman's terms, the scale space of a signal is the multiple low-frequency signals obtained by filtering the original signal with a series of single-parameter, increasing-width Gaussian filters. The explanation of the scale space theory is shown below:

Define $f(x)$ as a continuous function on the interval $[0, x_{max}]$ and $g(t)$ as a kernel function, the continuous scale space of the function can be expressed as:

$$L(x,t) = g(x;t) * f(x) \tag{15}$$

where t is the scale parameter, $*$ denotes the convolution operation.

The scale space can be interpreted as selecting different scale parameters to achieve varying levels of smoothing for the original function. When t is larger, the higher the degree of $L(x,t)$ smoothing, the less detail points are retained [22].

This paper explains the key function-based spectral trend estimation method based on the scale space theory. Assume $s(t)$ is a time domain signal, the amplitude spectrum $S(f)$ is obtained by performing a fast Fourier transform on $s(t)$.

$$S(f) = |FFT[s(t)]| \tag{16}$$

where FFT represents fast Fourier transform, $|\ \ |$ represents calculation of absolute value. $S(f)$ is a sequence of real numbers rather than a sequence of complex numbers.

Calculate the key function $K(u)$ of $S(f)$.

$$K(u) = FFT[S(f)] \tag{17}$$

Get the spectrum trend $T(m,f)$.

$$T(m,f) = IFFT[W(m;f) \cdot K(u)] \tag{18}$$

where $IFFT$ represents inverse fast Fourier transform, $W(m,f)$ represents the window function, m indicates the number of points reflecting the width of the window. The window function used in this paper is a rectangular window.

According to the convolution theorem, Eq. (17) can be written as:

$$T(m,f) = w(m;f) * S(f) \tag{19}$$

where $w(m;f) = IFFT[W(m;f)]$.

Defining different window lengths can get different spectrum trends. The longer the window, the finer the spectral trend; the more boundaries defined, the more bands are segmented; and vice versa, the fewer bands are segmented. The spectral trends corresponding to different values of m are represented in Fig. 4. Fig. 4(a) shows the simulation spectrum, Figs. 4(b), (c), (d)

show the spectral trends (solid yellow lines) obtained at $m = 10,15,25$, respectively, the red dashed lines in the Fig.4 indicate the boundary of the spectral division. Therefore, the window lengths from short to long can be defined to obtain multi-level spectrum segmentation results, and the segmentation process is adaptive, which improves the practicality of the spectrum segmentation method. The expression for the simulated signal is as follows:

$$\begin{cases} S_{c1}(t) = \sum_{k=1}^{50} e^{-2\pi\zeta_1 f_{n1} t} \cdot sin(2\pi f_{n1}\sqrt{1-\zeta_1^2}t)u(t-kT_1) \\ S_{c2}(t) = 10e^{-2\pi\zeta_2 f_{n2} t} \cdot sin(2\pi f_{n2}\sqrt{1-\zeta_2^2}t)u(t-0.45) \\ S_1(t) = S_{c1}(t) + S_{c2}(t) + g(t) \end{cases} \quad (20)$$

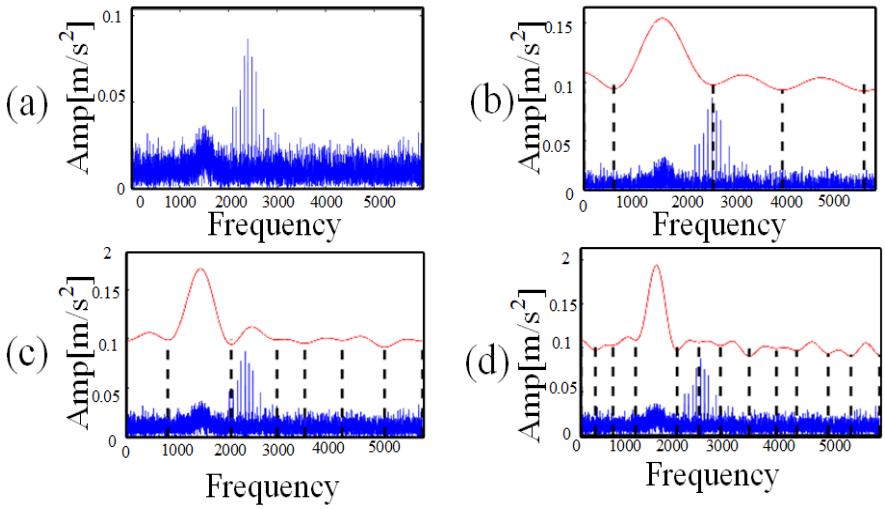

Fig.4. (a) Simulation spectrum; (b) Spectral trend at m=10; (c) Spectral trend at m=15; (d) Spectral trend at m=25;

where $S_{c1}(t)$ represents the periodic pulses and $S_{c2}(t)$ represents the incidental pulses at $t = 0.45s$,the inherent frequency $f_{n1} = 2400Hz, f_{n2} = 1500Hz$, damping ratio $\zeta_1 = 0.048$, damping ratio $\zeta_2 = 0.074$, pulse period $T_1 = 0.0125s$, i.e., the fault frequency $f_c = 80Hz$. To be more realistic, Gaussian white noise $g(t)$ with a SNR ratio of 4.1 dB is added.

Step 2: The empirical wavelet transform is used to decompose the raw signal into a series of empirical modal components. Find the location of the minimum in the spectrum trend obtained in Step 1 and filter the location of the minimum as the segmentation boundary. In this paper, the maximum number of levels is preset to beL_{max}, and the step size is $S = 5$， $m = S * L$.

Step 3: Calculate the LSES of all empirical modal components in each level. Iterate through all the empirical modal components and calculate the LSES, then draw the multi-level tower boundary schematic based on the LSES.

Step 4: Extract the frequency band with the largest LSES value, perform envelope analysis, extract the fault features in the envelop spectrum, and perform fault diagnosis.

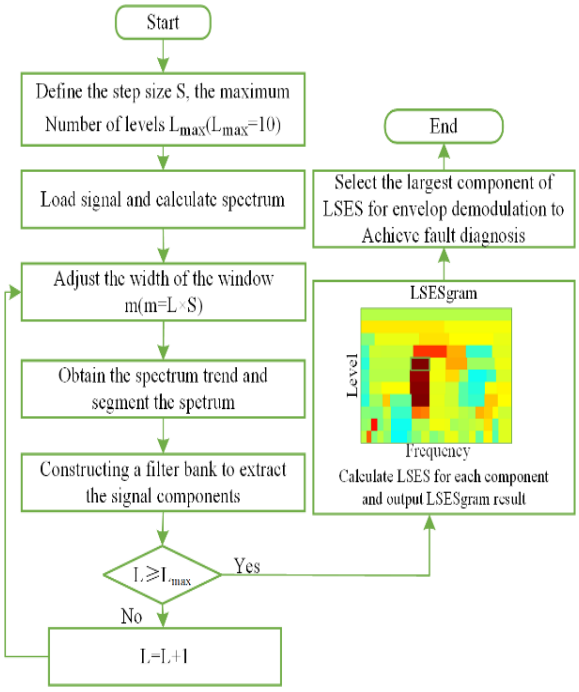

Fig. 5. The flow chart of LSESgram.

3. Simulation verification

In order to verify the effectiveness of the proposed method, this section constructs simulated signals based on (20) to simulate outer ring fault signals containing incidental pulses, and uses LSESgram for diagnosis.

The simulated signal $S_1(t)$ and its spectrum are shown in Fig.

6(a)-(b). In the time domain waveform, it can be clearly observed that the amplitude of the incidental pulse at 0.45s is much larger than the amplitude of other components in the signal, and it is difficult to observe the periodic pulse component in the time domain signal. Fig. 6(b) shows the frequency spectrum of the simulated signal.

LSESgram is used to process the signal, and the result is shown in Fig. 7(a). The signal is divided into 10 levels in the spectrum, and the band with the largest LSES value is located in level 4, with a bandwidth of 725 Hz and a center frequency of 2362.5 Hz, which is very close to the intrinsic frequency f_{n1}=2400Hz. The extracted frequency band and time domain waveforms are shown in Fig. 7(b), and their envelope spectra are shown in Fig. 7(c), where the fault characteristic frequency and its 2–6 harmonics can be clearly observed. Thus, it can be tentatively verified that LSESgram can still accurately and effectively extract the frequency band with the richest fault information when dealing with bearing fault signals containing incidental pulses. The simulated signal is as follows:

$$\begin{cases} s_1(t) = e^{-g\cdot 2\pi f_n t}\cdot sin\left(2\pi f_n\sqrt{1-g^2}\cdot t\right) \\ s_2(t) = 10\cdot e^{-\zeta\cdot 2\pi f_d\cdot mod\left(\frac{n}{Fs}-0.45,1/1\right)}\cdot sin\left(2\pi f_d\sqrt{1-\zeta^2}\cdot mod\left(\frac{n}{Fs}-0.45,1/1\right)\right) \\ s(t) = s_1(t)+s_2(t)+n(t) \end{cases} \tag{21}$$

Where $s_1(t)$ is periodic pulse, $s_2(t)$ is accidental pulse. natural frequency $f_n = 2400Hz$, $f_d = 1500Hz$, the damping cofficient $g = 0.048$, $\zeta = 0.074$. $n(t)$ represents white Gaussian noise with SNR of 4.3 dB.

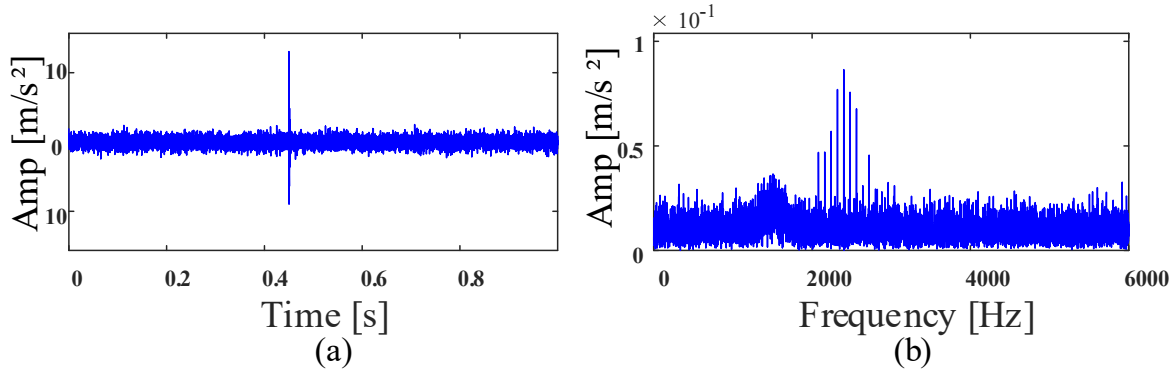

Fig. 6. (a)The time domain waveform of the simulated signal; (b) Its spectrum

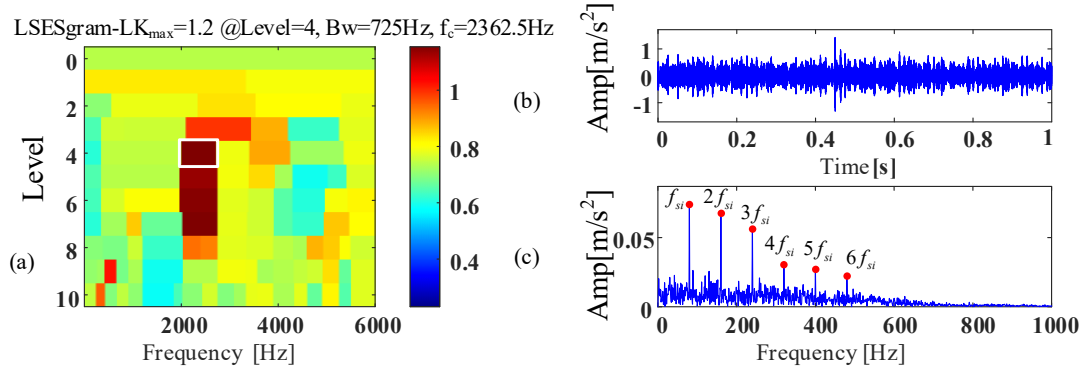

Fig. 7. LSESgram processing results of the simulated signal: (a) LSESgram; (b) The extracted component time domain waveform; (c) The envelope spectrum

4. Experimental verification

In order to demonstrate the effectiveness of LSESgram , two groups of experimental signals were processed simultaneously using LSESgram, Kurtogram, Infogram, Autogram, and the results were analyzed and compared

4.1. Experimental signal 1(bearing outer ring fault signal containing incidental pulse)

The bearing experimental signal comes from the HZXT-008

small rotor rolling bearing test stand, as shown in Fig. 8. The NSK-6200 deep groove ball bearing is used in the experiment.

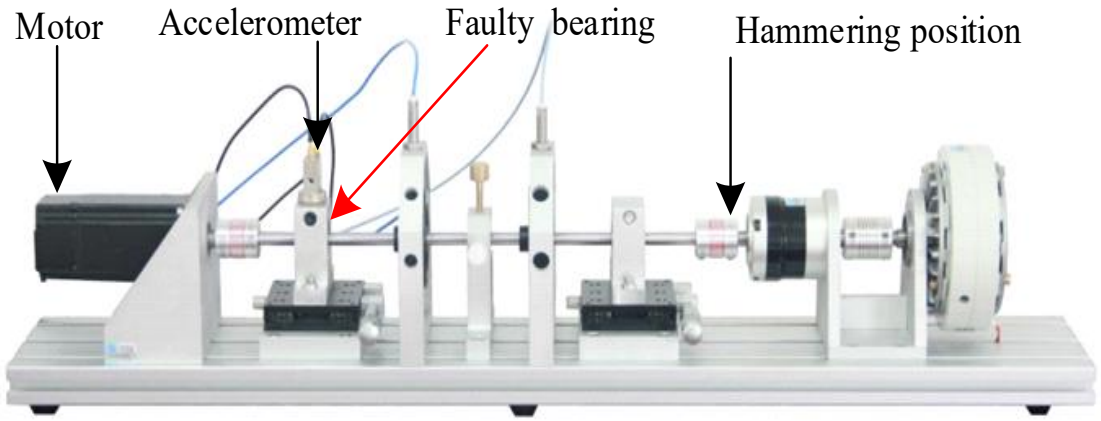

Fig. 8. The HZXT-008 small rotor rolling bearing test bench.

The sampling frequency $f_{s1} = 12000Hz$, the motor speed is set to 1500rpm, and the outer ring failure frequency is calculated to be $f_{o1} = 76.2$Hz.

To simulate the accidental pulse, a force hammer was used to strike the coupling in the outer ring failure experiment. The waveform, spectrum, and envelope of the acquired bearing outer ring fault signal containing the accidental pulse are shown in Figs. 9(b)-(c). A single incidental pulse of huge amplitude can be observed near $t = 0.33s$, and the periodic pulse in the original signal is not obvious. The envelope spectrum neither finds the characteristic frequency of the outer ring fault nor the more obvious harmonics, so it is difficult to find useful information to diagnose the fault.

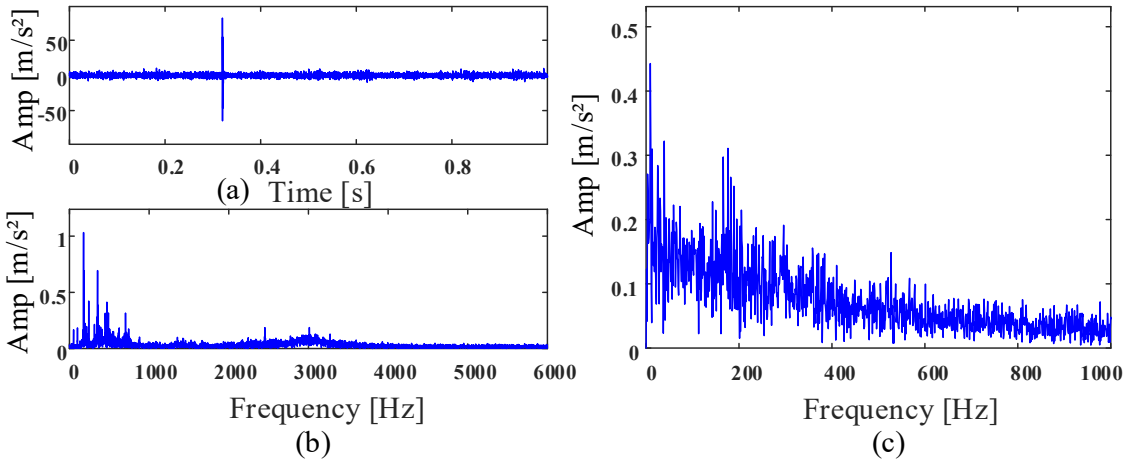

Fig. 9. (a) The time waveform of experimental signal 1. (b) Its spectrum. (c) Its envelope spectrum.

LSESgram is used to process signal 1, and the result is shown in Fig. 10(a). The bandwidth of the extracted band is 896Hz, the center frequency is 5552Hz, and the bandwidth range is [5104Hz, 6000Hz]. Fig. 10(b) shows the time-domain waveform of the extracted components. Although the time-domain waveform still contains the accidental pulse, the amplitude of the incidental pulses is significantly reduced compared with the original signal, and the periodic pulses are more obvious. Fig. 10(c) shows the envelope spectrum of the extracted components, and the outer ring fault characteristic frequency and its 2-7 harmonics can be clearly observed in the envelope spectrum, which can directly determine the bearing outer ring fault. Thus, it can be seen that LSESgram has good resistance to accidental pulse interference and can accurately identify and diagnose faults under interference, which proves the effectiveness of LSESgram.

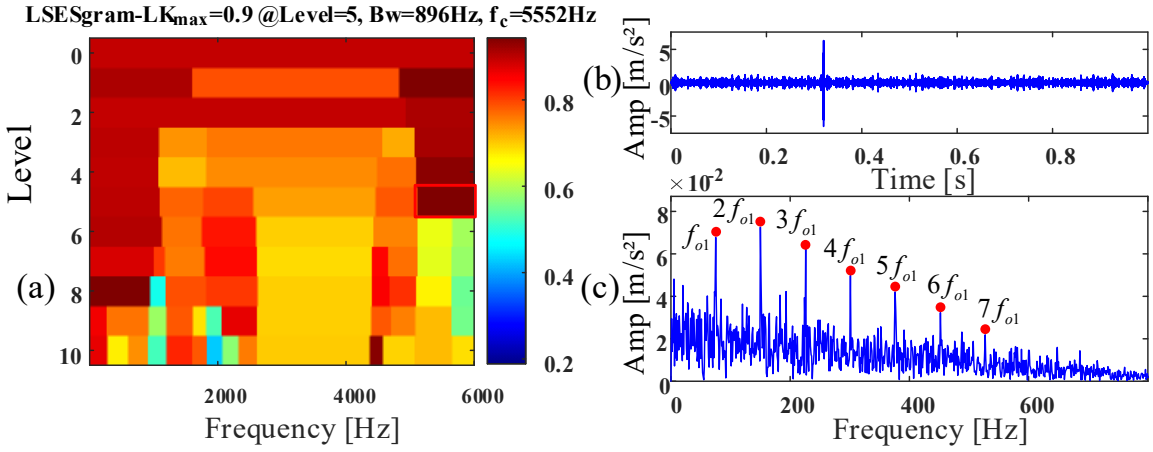

Fig. 10. LSESgram processing results of the experimental signal 1: (a) LSESgram; (b) The extracted component time domain waveform; (c) The envelope spectrum.

Fast Kurtogram is used to process the signal 1. Fig. 11(a) shows the result of Kurtogram. The center frequencies of the extracted band are 3000 Hz, the bandwidth is 2000 Hz, and the bandwidth range is [2000, 4000] Hz. Fig. 11(b) shows the time domain waveform of the extracted component which contains an accidental pulse and the amplitude of this accidental pulse is quite close to the amplitude of the accidental pulse in the original signal. Fig. 11(c) shows the envelope spectrum of the extracted component, only the 4-5 harmonics of the characteristic frequency of the fault can be roughly observed in the envelope spectrum, and no further information is available. This also shows that Fast Kurtogram is more sensitive to chance pulses and fails easily when processing signals containing chance pulses.

Infogram is used to process the signal 1 and the results are shown in Fig. 12(a), Fig. 13(a), and Fig. 14(a). Only the results obtained by SE Infogram are similar to those obtained by LSESgram, SES Infogram does not extract fault information, and the results of the Average Infogram only showing the 4th-5th harmonics of the fault characteristic frequency, with limited fault information. Further comparing the results of LSESgram with those of SE Infogram, it can be seen that SE Infogram extracts a wider frequency band, which leads to more noise being included in the envelope spectrum, and the envelope spectrum of the components extracted by LSESgram has less noise and the fault characteristic frequencies and their harmonics are more pronounced.

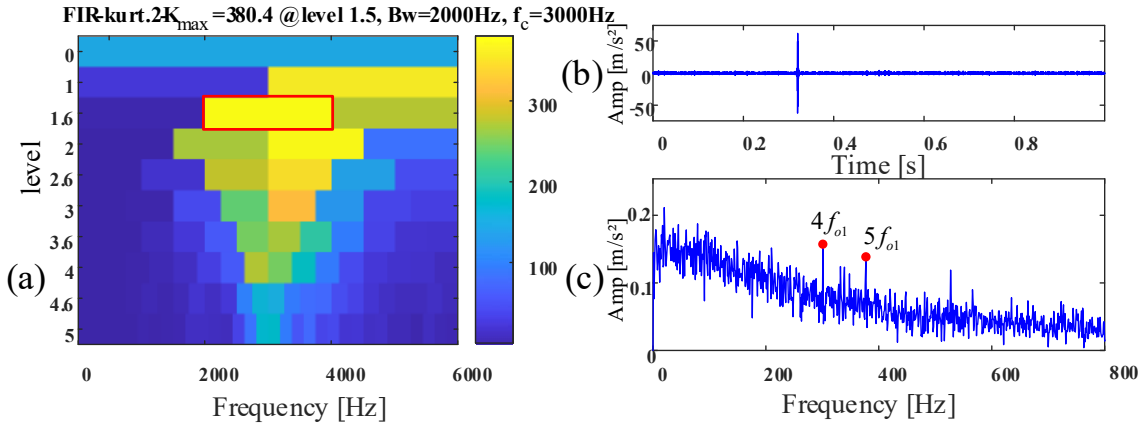

Fig. 11. Fast Kurtogram processing results of the experimental signal 1: (a) Fast Kurtogram; (b) The extracted component time domain waveform; (c) The envelope spectrum.

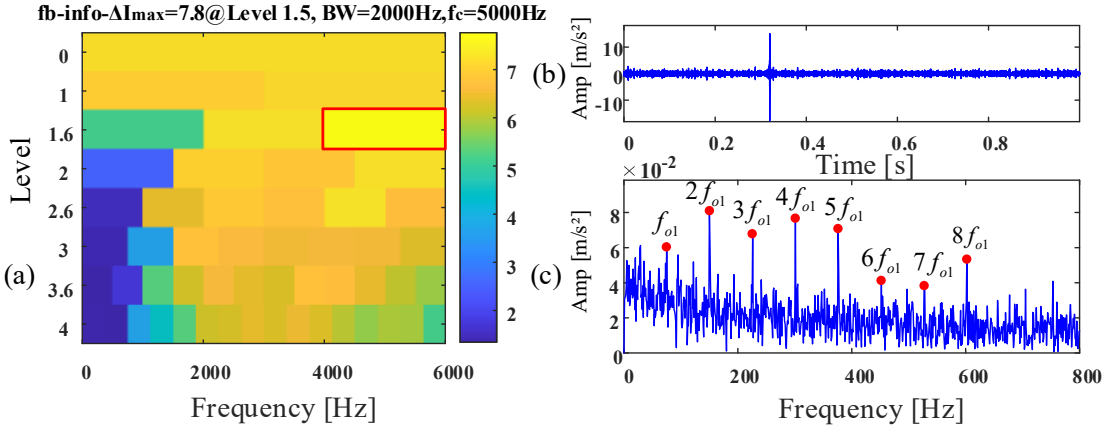

Fig. 12. SE Infogram processing results of the experimental signal 1: (a) SE Infogram; (b) The extracted component time domain waveform; (c) The envelope spectrum.

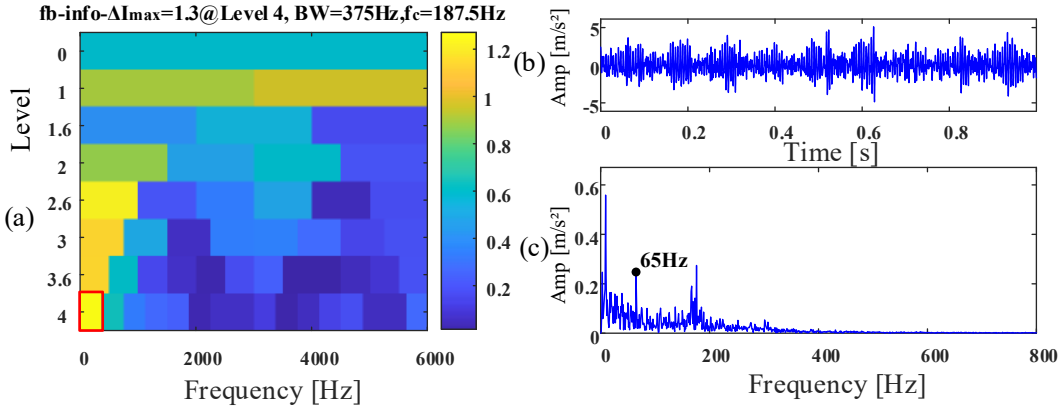

Fig. 13. SES Infogram processing results of the experimental signal 1: (a) SES Infogram; (b) The extracted component time domain waveform; (c) The envelope spectrum.

Autogram is used to process the signal 1, and the result is shown in Fig. 15(a). The extracted band bandwidth is 375Hz, the center frequency is 1687.5H, and the bandwidth range is [1500Hz, 1875Hz]. Autogram extracted components can neither find more obvious periodic pulse characteristics from the waveform nor is the outer ring fault frequency or harmonics observed in the envelope spectrum (the highest spectral line represents a frequency of 82Hz, which has a large error with the fault characteristic frequency). Therefore, the kurtosis of the unbiased autocorrelation of the squared envelope of the demodulation signal does not completely eliminate the effect of chance pulses.

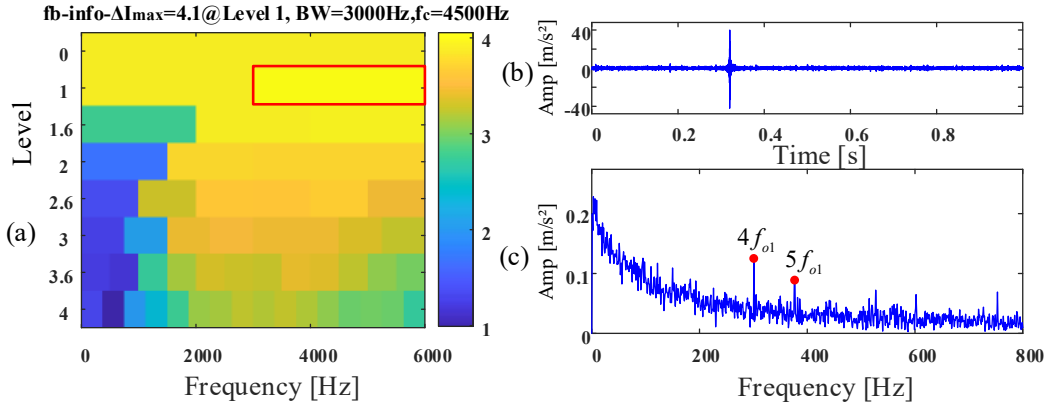

Fig. 14. Average Infogram processing results of the experimental signal 1: (a) Average Infogram; (b) The extracted component time domain waveform; (c) The envelope spectrum.

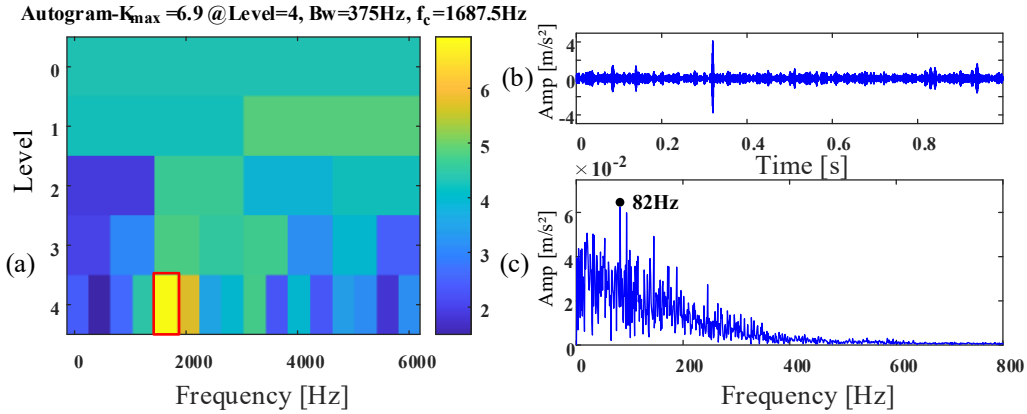

Fig. 15. Autogram processing results of the experimental signal 1: (a) Autogram; (b) The extracted component time domain waveform; (c) The envelope spectrum.

4.2. Experimental signal 2 (bearing inner ring fault signal containing harmonic interference)

In order to further verify the suppression ability of the proposed LSESgram on the irrelevant harmonic components in the bearing fault vibration signal and the extraction ability of the periodic pulse components, a rolling bearing fault simulation experiment was completed on the QPZZ bearing fault simulation test bench, the structure of the experimental platform is shown in Fig. 16, and the N205 bearing is used for the experiment, and the displacement vibration signal is collected by the electric

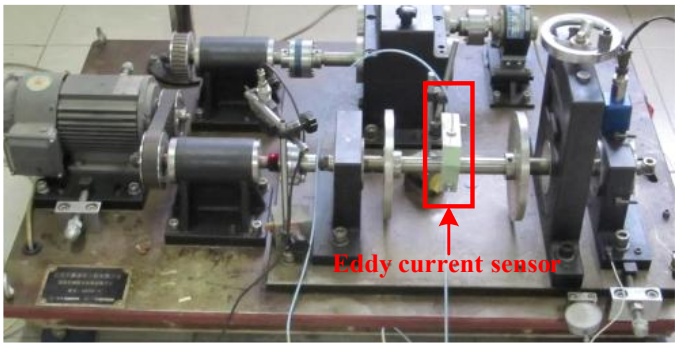

Fig. 16. The QPZZ bearing fault simulation test bench.

The displacement vibration signal is collected by the eddy current sensor installed on the shaft. The sampling frequency f_{s2} = 12800Hz, the motor speed is 1440r/min, and the outer ring fault characteristic frequency f_{o2} = 116Hz. Fig. 17(a)-(c) shows the waveform, spectrum, and envelope spectrum of the outer ring fault signal with harmonic interference. Harmonic features can be clearly observed in the signal waveform, which is the result of strong harmonic interference. Further observation of the spectrum shows that the side frequency band is mainly concentrated between [500, 1800] Hz, and the low-frequency region is dominated by the harmonics of the rotational frequency, where the amplitude of rotation frequency at 24 Hz is much larger than other frequency components, which makes some statistical indicators calculated in the frequency domain tend to maximize, thus interfering with the determination of the center frequency and bandwidth of the frequency band where the fault is located, which is not conducive to obtaining fault information.

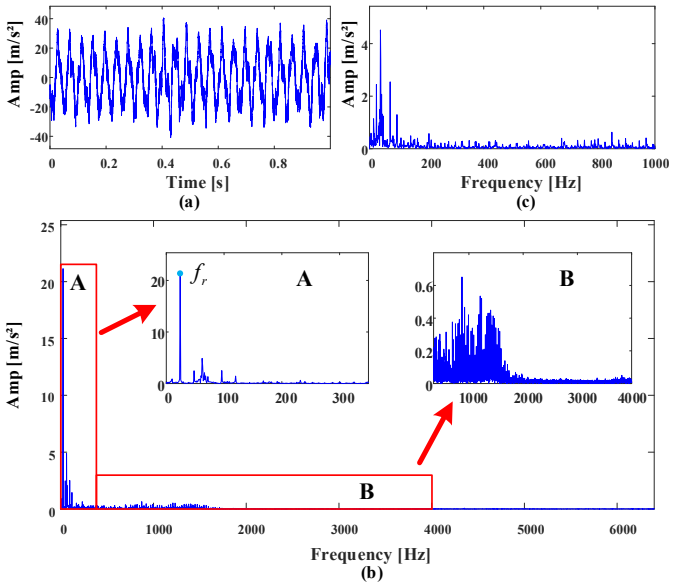

Fig.17. (a) The time waveform of experimental signal 2. (b) Its spectrum. (c) Its envelope spectrum.

LSESgram is used to process the signal 2, and the result is shown in Fig. 18(a). The bandwidth of the extracted band is 1648 Hz, the center frequency is 2909 Hz, and the bandwidth range is [2085, 3733] Hz. Fig. 18(b) shows the time domain waveform of the extracted component, where the harmonic form is not present in the time domain waveform and the

periodic pulses are highlighted. Fig. 18(c) shows the envelope spectrum of the extracted components, which contains the rotational frequency, also the outer ring fault characteristic frequency and its 2-8 harmonics can be clearly observed, thus it can be directly determined that the outer ring of this bearing is faulty, and it also shows that the LSESgram is still valid even if there is a strong harmonic interference phenomenon in the signal.

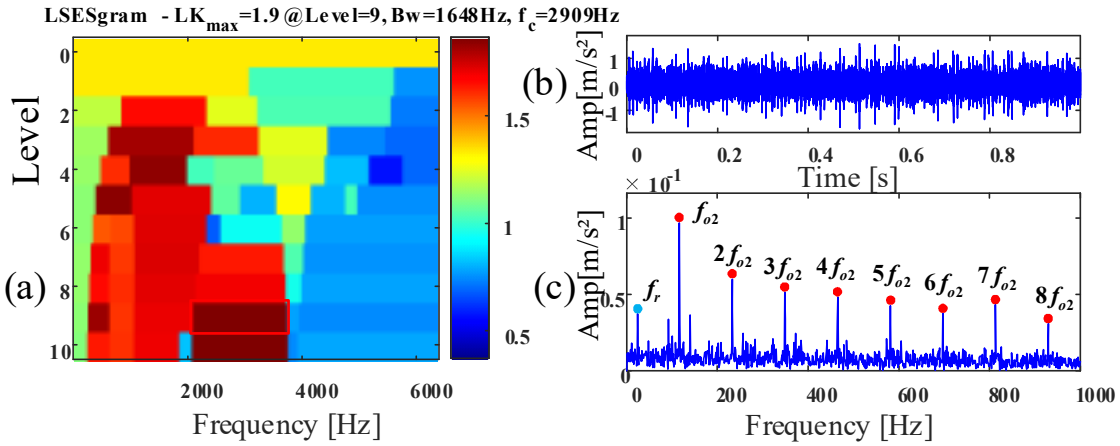

Fig. 18. LSESgram processing results of the experimental signal 3: (a) LSESgram; (b) The extracted component time domain waveform; (c) The envelope spectrum.

The signal 2 was processed using Fast Kurtogram, and the result is shown in Fig. 19(a). The center frequency of the band extracted is around 1800 Hz, and the bandwidth is 533.3 Hz. The time domain waveform and the envelope spectrum are shown in Fig. 19(b)-(c). Although there are periodic pulses in the time-domain waveforms, the envelope spectrum mainly shows the 2nd and higher harmonics of rotational frequency. Fault characteristic frequency and its 2nd harmonic are hidden and difficult to be directly observed.

Infogram is used to process the signal 2, and the results are shown in Fig. 20(a), Fig. 21(a), and Fig. 21(b). The result obtained by the SE Infogram is similar to the result obtained by Fast Kurtogram. Both SES Infogram and Average Infogram select the whole spectrum of the signal 2, which indicates that the strong harmonic interference directly affects the calculation of the spectral negentropy and the average spectral negentropy of the frequency domain spectrum, leading to the failure of the two methods.

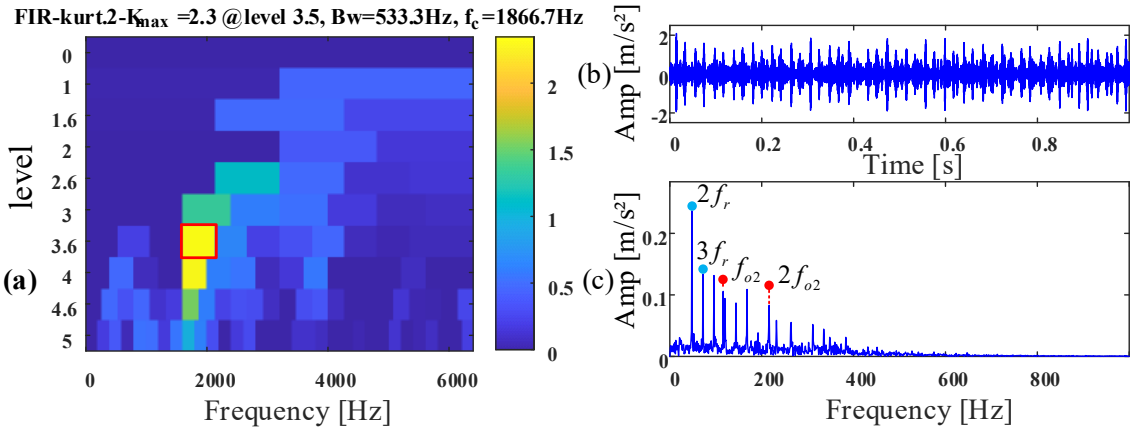

Fig. 19. Fast Kurtogram processing results of the experimental signal 3: (a) Fast Kurtogram; (b) The extracted component time domain waveform; (c) The envelope spectrum.

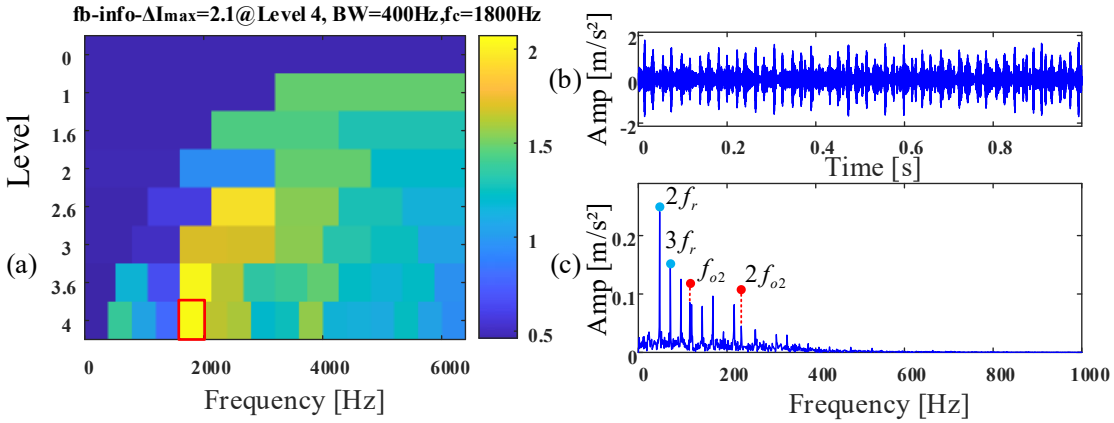

Fig.20. SE Infogram processing results of the experimental signal 3: (a) SE Infogram; (b) The extracted component time domain waveform; (c) The envelope spectrum.

Autogram is used to process the signal 2, and the result is shown in Fig. 22(a). The result obtained by Autogram is the same as the result obtained by the SE Infogram, and it is difficult to obtain valid fault information.

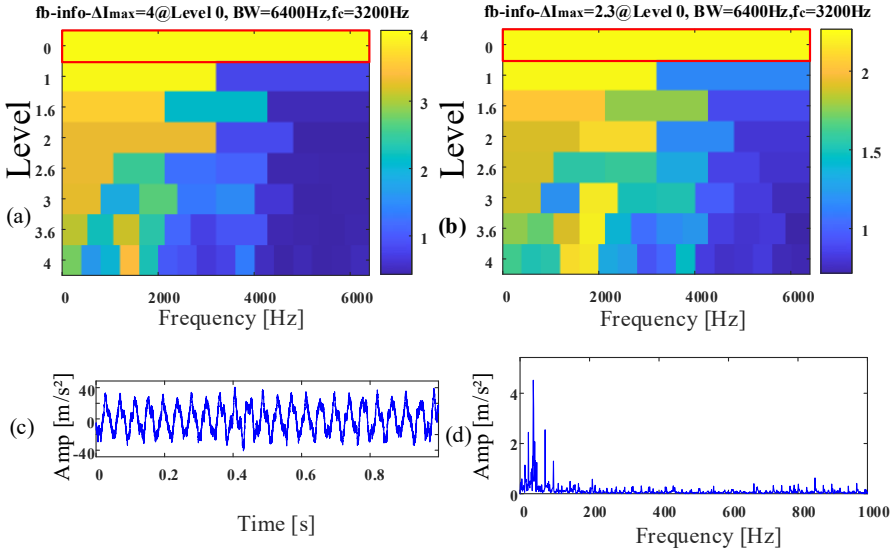

Fig. 21. SES Infogram and Average Infogram processing results of the experimental signal 3: (a) SES Infogram; (b) Average Infogram; (c) The extracted component time domain waveform; (d) The envelope spectrum.

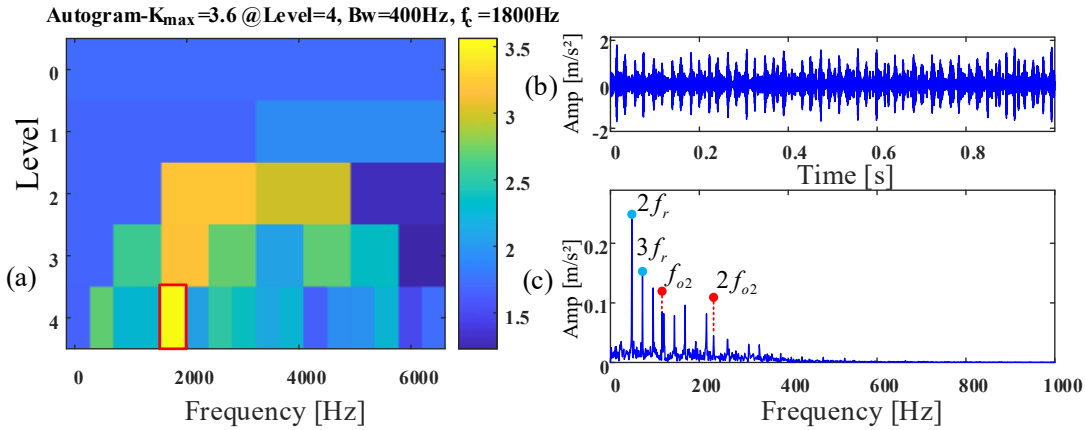

Fig.22 Autogram processing results of the experimental signal 2: (a) Autogram; (b) The extracted component time domain waveform; (c) The envelope spectrum.

5. Conclusion

This paper proposes an optimal demodulation band extraction method, LSESgram, which can resist stronger noise and is free from chance shocks and irrelevant harmonic interference. Multi-stage spectrum segmentation based on spectrum trend can be combined with the spectral shape of the signal to make a more reasonable and effective division of the spectrum, which is more adaptive and practical. The use of a new indicator, the LSES indicator, can avoid accidental shocks and irrelevant harmonic interference and can discover the periodic components in the signal in the case of strong noise.

In this paper, the effectiveness of the method is demonstrated by constructing one set of simulated signals and comparing LSESgram with Fast Kurtogram, Infogram, and Autogram with the help of three sets of experimental signals. LSESgram can discover more accurate center frequencies and more suitable bandwidths compared with other methods, so that the obtained signal components contain richer fault information, and thus more accurate fault diagnosis results can be obtained. Therefore, LSESgram can be applied to bearing fault diagnosis.

Our next work will focus on applying LSES to neural networks as input data for artificial intelligence algorithms and attempting to design an online fault diagnosis system.

References

1. R. B. Randall, and J. Antoni, "Rolling element bearing diagnostics-A tutorial," Mech. Syst. Signal Proc., vol. 25, no. 2, pp. 485-520, Feb. 2011.https://doi.org/10.1016/j.ymssp.2010.07.017
2. M. Yang, K. Zhang Z. Sheng, X. Zhang and Y. Xu, "The amplitude modulation bispectrum: A weak modulation features extracting method for bearing fault diagnosis," Reliab. Eng. Syst. Saf., vol. 250, Oct. 2024. https://doi.org/10.1016/j.ress.2024.110241
3. H. Wang, S. Li, L. Song and L. Cui, "A novel convolutional neural network based fault recognition method via image fusion of multi-vibration-signals," Comput. Ind., vol. 105, pp. 182-190, Feb 2019.https://doi.org/10.1016/j.compind.2018.12.013
4. X. Zou, H. Zhang, Z. Jiang, K. Zhang and Y. Xu, "Toward accurate extraction of bearing fault modulation characteristics with novel time-frequency modulation bispectrum and modulation Gini index analysis," Mech. Syst. Signal Proc., vol. 219, no. 1, Oct. 2024.https://doi.org/10.1016/j.ymssp.2024.111629
5. C. Ma, C. Liang, Z. Jiang, K. Zhang and Y. Xu, "A novel time-frequency slice extraction method for target recognition and local enhancement of non-stationary signal features," ISA T., vol. 146, pp. 319-335, Mar. 2024. https://doi.org/10.1016/j.isatra.2024.01.003
6. W. Huo, Z. Jiang, Z. Sheng, K. Zhang and Y. Xu, "Cyclostationarity blind deconvolution via eigenvector screening and its applications to the condition monitoring of rotating machinery," Mech. Syst. Signal Proc., vol. 222, no. 1, Jan. 2005. https://doi.org/10.1016/j.ymssp.2024.111782
7. Y.T. Sheen, "An envelope analysis based on the resonance modes of the mechanical system for the bearing defect diagnosis," Measurement, vol. 43, no. 7, pp. 912-934, Aug. 2010.https://doi.org/10.1016/j.measurement.2010.03.011
8. Q. Tian; C. Hou and S. Li, "Adaptive resonant demodulation for early fault diagnosis of ball bearing," IEEE China Summit & International Conference on Signal and Information Processing, Beijing, China, Jul. 06-10, 2013. https://doi.org/10.1109/ChinaSIP.2013.6625292
9. R. Dwyer, "Detection of non-Gaussian signals by frequency domain Kurtosis estimation," International Conference on Acoustics, Speech, and Signal Processing, Boston, MA, USA, Apr. 14-16, 1983.
10. J. Antoni, "The spectral kurtosis: a useful tool for characterising non- stationary signals," Mech. Syst. Signal Proc., vol. 20, no. 2, pp. 282-307, Feb. 2006.https://doi.org/10.1016/j.ymssp.2004.09.001
11. J. Antoni, and R.B. Randall, "The spectral kurtosis: application to the vibratory surveillance and diagnostics of rotating machines," Mech. Syst. Signal Proc., vol. 20, no. 2, pp. 308-331, Feb. 2006.https://doi.org/10.1016/j.ymssp.2004.09.002
12. J. Antoni, "Fast computation of the kurtogram for the detection of transient faults," Mech. Syst. Signal Proc., vol. 21, no. 1, pp. 108-124, Feb. 2007.https://doi.org/10.1016/j.ymssp.2005.12.002
13. P. Borghesani and J. Antoni, "CS2 analysis in presence of non-Gaussian background noise - Effect on traditional estimators and resilience of log-envelope indicators," Mech. Syst. Signal Proc., vol. 90, pp. 378-398, Jun. 2017. https://doi.org/10.1016/j.ymssp.2016.12.033
14. Y. Lei, J. Lin, Z. He and Y. Zi, "Application of an improved kurtogram method for fault diagnosis of rolling element bearings," Mech. Syst. Signal Proc., vol. 25, no. 5, pp. 1738-1749, Jul. 2011.https://doi.org/10.1016/j.ymssp.2010.12.011
15. T. Barszcz and A. Jablonski, "A novel method for the optimal band selection for vibration signal demodulation and comparison with the Kurtogram," Mech. Syst. Signal Proc., vol. 25, no. 1, pp. 431-451, Jan. 2011. https://doi.org/10.1016/j.ymssp.2010.05.018
16. D. Wang, Y. Zhao, C. Yi, K. Tsui and J. Lin, "Sparsity guided empirical wavelet transform for fault diagnosis of rolling element bearings," Mech. Syst. Signal Proc., vol. 101, no. 15, pp. 292-308, Feb. 2018. https://doi.org/10.1016/j.ymssp.2017.08.038
17. P. Tse and D. Wang, "The design of a new sparsogram for fast bearing fault diagnosis: Part 1 of the two related manuscripts that have a joint title as "Two automatic vibration-based fault diagnostic methods using the novel sparsity measurement - Parts 1 and 2"," Mech. Syst. Signal Proc., vol. 40, no. 2, pp. 499-519, Nov. 2013. https://doi.org/10.1016/j.ymssp.2013.05.024

18. J. Antoni, "The infogram: Entropic evidence of the signature of repetitive transients," Mech. Syst. Signal Proc., vol. 74, no. 1, pp. 73-94, Jun. 2016.https://doi.org/10.1016/j.ymssp.2015.04.034
19. A. Moshrefzadeh and A. Fasana, "The Autogram: An effective approach for selecting the optimal demodulation band in rolling element bearings diagnosis," Mech. Syst. Signal Proc., vol. 105, no. 15, pp. 294-318, May 2018. https://doi.org/10.1016/j.ymssp.2017.12.009
20. X. Wang, J. Zheng, Q. Ni, H. Pan and J. Zhang, "Traversal index enhanced-gram (TIEgram): A novel optimal demodulation frequency band selection method for rolling bearing fault diagnosis under non-stationary operating conditions," Mech. Syst. Signal Proc., vol. 172, no. 1, pp. 109017, Jun. 2022. https://doi.org/10.1016/j.ymssp.2022.109017
21. J. R. M. Hosking, "L-moments: analysis and estimation of distributions using linear combinations of order statistics," J. R. Stat. Soc. Ser. B-Methodol., vol. 52, no. 1, pp. 105-124, Sep. 1990.https://doi.org/10.1111/j.2517-6161.1990.tb01775.x
22. J. Gilles and K. Heal, "A parameterless scale-space approach to find meaningful modes in histograms - Application to image and spectrum segmentation," Int. J. Wavelets Multiresolut. Inf. Process., vol. 12, no. 6, Nov. 2014. https://doi.org/10.1142/S0219691314500441